

An efficiency and memory-saving programming paradigm for the unified gas-kinetic scheme

Yue Zhang^a, Yufeng Wei^a, Wenpei Long^a, Kun Xu^{a,b,c,*}

^a*Department of Mathematics, Hong Kong University of Science and Technology, Clear Water Bay, Kowloon, Hong Kong*

^b*Department of Mechanical and Aerospace Engineering, Hong Kong University of Science and Technology, Clear Water Bay, Kowloon, Hong Kong*

^c*Shenzhen Research Institute, Hong Kong University of Science and Technology, Shenzhen, China*

Abstract

In recent years, non-equilibrium flows have gained significant attention in aerospace engineering and micro-electro-mechanical systems. The unified gas-kinetic scheme (UGKS) follows the methodology of direct modeling to couple particle collisions and free transport during gas evolution. However, like other discrete-velocity-based methods, the UGKS faces challenges related to high memory requirements and computational costs, such as the possible consumption of 1.32 TB of memory when using 512 cores for the simulations of the hypersonic flow around an X38-like space vehicle. This paper introduces a new UGKS programming paradigm for unstructured grids, focusing on reducing memory usage and improving parallel efficiency. By optimizing the computational sequence, the current method enables each cell in physical space to store only the distribution function for the discretized velocity space, eliminating the need to retain the entire velocity space for slopes and residuals. Additionally, the parallel communication is enhanced through the use of non-blocking MPI. Numerical experiments demonstrate that the new strategy in the programming effectively simulates non-equilibrium problems while achieving high computational efficiency and low memory consumption. For the hypersonic flow around an X38-like space vehicle, the simulation, which utilizes 1,058,685 physical mesh cells and 4,548 discrete velocity space mesh cells, requires only 168.12 GB of memory when executed on 512 CPU cores. This indicates that memory consumption in the UGKS is much reduced. This new programming paradigm can serve as a reference for discrete velocity methods for solving kinetic equations.

Keywords:

Unified Gas-Kinetic Scheme, Reduce memory usage, High computational efficiency, Non-blocking MPI

*Corresponding author

Email addresses: y Zhang@connect.ust.hk (Yue Zhang), yweibe@connect.ust.hk (Yufeng Wei), wlongab@connect.ust.hk (Wenpei Long), makxu@ust.hk (Kun Xu)

1. Introduction

Multiscale flows are commonly encountered in applications of aerospace engineering and micro-electro-mechanical systems (MEMS). For high-speed flying vehicles, the highly compressed gas at the leading edge and the strong expansion wave in the trailing edge can cover the whole flow regimes [1, 2]. In MEMS, the small size of the structure and the low pressure of the encapsulation result in significant rarefaction effects of gas [3, 4, 5, 6]. Therefore, developing an efficient and accurate multiscale simulation program is very important.

For multiscale flows across all Knudsen regimes, the description of particle collisions and free streaming are equally important. Accurately capturing non-equilibrium physics requires more degrees of freedom which are provided in the kinetic formulation. The Boltzmann equation is the fundamental governing equation in rarefied gas dynamics. Theoretically, it can capture multiscale flow physics in all Knudsen regimes, with the enforcement of resolving the flow physics in the particle mean free path and collision time scale. Mainstream computational methods of solving non-equilibrium flows can be divided into stochastic and deterministic approaches. The stochastic methods employ stochastic particles to simulate the statistical behavior of molecular gas dynamics, and the direct simulation Monte Carlo (DSMC) method [7, 8, 9] is the most popular, which uses probabilistic Monte Carlo simulation to solve the Boltzmann equation. This method characterizes the non-equilibrium physics through particles within local velocity space, achieving high computational efficiency for hypersonic rarefied flow. During the gas evolution process, particles' free streaming and collision strictly follow conservation law, guaranteeing high robustness. However, its stochastic nature of particles introduce statistical noise. In low-speed flow simulations, the method requires many particles or multiple statistical averaging to reduce the noise. Meanwhile, the computational cost of solving intensive partial collisions in the continuum flow regime is very high. Deterministic methods like the discrete velocity method (DVM) [10, 11, 12, 13] use the discrete velocity distribution function to solve the Boltzmann equation with different models. In the deterministic method, the gas evolution flux on the cell interface is often required to be constructed based on the same velocity space. Therefore, an accurate solution with no statistical noise can be obtained. However, the global velocity space brings massive memory consumption and computational cost, especially for three-dimensional high-speed flow simulations. In both stochastic and deterministic methods, when the solution of the kinetic model is split into particle-free streaming and instant collision, numerical dissipation that is proportional to the timestep often becomes inevitable. Consequently, with the splitting treatment, the mesh size and time step must be smaller than the particle mean free path and mean collision time, respectively. This ensures that the numerical dissipation in the continuum flow regime does not overshadow the physical dissipation.

In recent years, gas-kinetic methods, such as the DVM-based unified gas-kinetic scheme (UGKS) [14, 15], the particle-based unified wave-particle (UGKWP) method [16, 17], discrete UGKS (DUGKS) [18] and discrete UGKWP method [19] are proposed. With the coupled particle collisions and free transport in gas evolution, these methods release the constraints on the mesh size and time step for accurate solution in different regime, which is specifically effective in the regime with intensive particle collisions. These methods have

been further developed to consider real gas effects by introducing heat flux modification [20], rotational models [21], and vibrational models [22, 23]. They have been applied in various systems, including microflow [24, 25], compressible flow [26, 27], binary gas mixture [28], radiation transfer [29, 30], plasma [31], radiative plasma [32], neutron transport [33], phonon transport [34], and electron-phonon coupling heat transfer [35]. At the same time, the multiscale particle methods have been constructed as well [36, 37]. All these multiscale methods have the unified preserving (UP) property in capturing the Navier-Stokes solution in the continuum regime [38].

Recently, numerous efforts have been made to enhance DVM-based algorithms, such as UGKS and DUGKS, for industrial applications by accelerating performance and reducing memory consumption. One notable memory reduction technique involves the introduction of an unstructured discrete velocity space (DVS) [39], which significantly decreases the velocity space mesh in three-dimensional problems without compromising accuracy. The adaptive UGKS (AUGKS) [40] employs an adaptive velocity space decomposition to capture the non-equilibrium parts of the flow field, utilizing a discrete distribution function in corresponding areas while applying a continuous distribution function in others. This approach effectively conserves memory in near-continuous flow regimes. The performance of AUGKS in three-dimensional flows with rotational and vibrational non-equilibrium was further improved [41]. Adaptive methods such as the adaptive DUGKS [42] and the adaptive UGKWP [43] have also been proposed. Regarding acceleration, several studies have integrated implicit methods into UGKS. The implicit UGKS has been developed for both steady [44] and unsteady [45] solutions, achieving convergence that is 1 to 2 orders of magnitude faster than explicit UGKS across all flow regimes by combining macroscopic predictions with microscopic implicit iterations. The IUGKS has been extended to three-dimensional thermal non-equilibrium flows, accounting for rotational and vibrational degrees of freedom [46]. Recently, the IAUGKS [47] was introduced, combining these advanced techniques. In addition, other numerical techniques, such as reduce dimension by axisymmetric [48], high-order/low-order (HOLO) methods [49, 50], memory reduction techniques [51, 52], fast evaluation of the full Boltzmann collision term [53, 54], and adaptive refinement method [55], can be also used to accelerate the deterministic method.

In the present work, we aim to improve the performance of UGKS by designing a new programming paradigm rather than focusing solely on algorithmic enhancements. Hybrid parallel algorithms based on MPI/OpenMP have been designed [56, 57, 58], where MPI is used for parallelism in physical space and OpenMP in velocity space. However, due to OpenMP's relatively low parallel efficiency and the significant memory consumption in velocity space, it is challenging to apply these methods in large-scale computations. Subsequently, researchers [59, 60, 61, 62, 63] implemented MPI parallelism in both physical and velocity spaces, which reduces the memory requirements for individual cores, allowing the UGKS to tackle larger-scale problems. Nonetheless, MPI parallelism in velocity space often involves reduction operations, leading to lower parallel efficiency. The main goal of this paper is to design a program framework for the UGKS that requires less memory and achieves higher parallel efficiency. First, the paper analyzes the UGKS to minimize the storage requirements in velocity space. For parallelism, the approach focuses solely on physical space but

communicates point by point in velocity space to reduce the amount of data exchanged in each communication step. The framework maintains high parallel efficiency by combining this with non-blocking communication.

The organization of this paper is as follows. The basic model and formulation of the UGKS are presented in section 2. Section 3 introduces the designation of the code, including memory usage and parallelization of the method. Several test cases, including a three-dimensional cavity and hypersonic flow around a cylinder, a sphere, and an X38-like vehicle, are presented in section 4. In addition, the computation performance is also discussed in this section. Finally, section 5 concludes the paper and outlines potential future work.

2. Unified Gas-Kinetic Scheme

2.1. The BGK-Shakhov model

The basic model is the BGK-Shakhov equation,

$$\frac{\partial f}{\partial t} + \mathbf{u} \cdot \nabla f = \frac{f^+ - f}{\tau}, \quad (1)$$

where $f = f(\mathbf{x}, t, \mathbf{u}, \boldsymbol{\xi})$ is the distribution function for gas molecules at physical space location \mathbf{x} with microscopic translation velocity \mathbf{u} and internal velocity $\boldsymbol{\xi}$, τ is particle collision time, and f^+ is the modified equilibrium distribution function. The modified equilibrium distribution function is given by

$$f^+ = g \left[1 + (1 - \text{Pr}) \mathbf{c} \cdot \mathbf{q} \left(\frac{c^2}{RT} - 5 \right) / (5pRT) \right] = g + g^+,$$

where g is the Maxwellian distribution, Pr is the Prandtl number, $\mathbf{c} = \mathbf{u} - \mathbf{U}$ is the random velocity, \mathbf{U} is the macroscopic velocity, \mathbf{q} is the heat flux, R is gas constant and T is the temperature. The Maxwellian distribution is

$$g = \rho \left(\frac{\lambda}{\pi} \right)^{\frac{K+D}{2}} e^{-\lambda((\mathbf{u}-\mathbf{U})^2 + \boldsymbol{\xi}^2)},$$

where ρ is density, $\lambda = m/(2k_B T)$, m is molecule mass, k_B is Boltzmann constant, D is the spatial dimension, K is the number of internal degrees of freedom and $\boldsymbol{\xi}^2 = \xi_1^2 + \xi_2^2 + \dots + \xi_K^2$.

The collision terms meet the requirement of conservative constraint or compatibility condition

$$\int (f^+ - f) \Psi \, d\mathbf{u} \, d\boldsymbol{\xi},$$

where $\Psi = (1, \mathbf{u}, \frac{1}{2}(\mathbf{u}^2 + \boldsymbol{\xi}^2))^T$ is the collision invariants and $d\boldsymbol{\xi} = d\xi_1 d\xi_2 \dots d\xi_K$. The

macroscopic variables can be calculated via

$$\mathbf{W} = \begin{pmatrix} \rho \\ \rho \mathbf{U} \\ \rho E \end{pmatrix} = \int \Psi f \, d\mathbf{u} \, d\boldsymbol{\xi},$$

$$\mathbf{q} = \frac{1}{2} \int (\mathbf{u} - \mathbf{U})(|\mathbf{u} - \mathbf{U}|^2 + \boldsymbol{\xi}^2) f \, d\mathbf{u} \, d\boldsymbol{\xi}.$$

2.2. Reduced distribution function

To reduce memory usage, we introduce two reduced distribution functions h and b , defined by

$$h(\mathbf{x}, t, \mathbf{u}) = \int f \, d\boldsymbol{\xi},$$

$$b(\mathbf{x}, t, \mathbf{u}) = \int \boldsymbol{\xi}^2 f \, d\boldsymbol{\xi},$$

By multiplying Eq.(1) by 1 and $\boldsymbol{\xi}^2$ and integrating over the inner degrees, we can obtain

$$\begin{aligned} \frac{\partial h}{\partial t} + \mathbf{u} \cdot \nabla h &= \frac{h^+ - h}{\tau}, \\ \frac{\partial b}{\partial t} + \mathbf{u} \cdot \nabla b &= \frac{b^+ - b}{\tau}, \end{aligned} \tag{2}$$

where the reduced equilibrium distributions are

$$\begin{aligned} h^+ &= H + H^+, \\ b^+ &= B + B^+. \end{aligned}$$

The corresponding reduced Maxwellian distribution g becomes,

$$\begin{aligned} H &= \int g \, d\boldsymbol{\xi} = \rho \left(\frac{\lambda}{\pi} \right)^{D/2} e^{-\lambda(\mathbf{u}-\mathbf{U})^2}, \\ B &= \int \boldsymbol{\xi}^2 g \, d\boldsymbol{\xi} = \frac{3-D+K}{2\lambda} H, \end{aligned}$$

and the corresponding terms related to g^+ becomes

$$\begin{aligned} H^+ &= \int g^+ \, d\boldsymbol{\xi} = \frac{4(1-Pr)\lambda^2}{5\rho} (\mathbf{u} - \mathbf{U}) \cdot \mathbf{q} (2\lambda(\mathbf{u} - \mathbf{U})^2 - 2 - D) H, \\ B^+ &= \int \boldsymbol{\xi}^2 g^+ \, d\boldsymbol{\xi} = \frac{4(1-Pr)\lambda^2}{5\rho} (\mathbf{u} - \mathbf{U}) \cdot \mathbf{q} \{ [2\lambda(\mathbf{u} - \mathbf{U})^2 - D](3 - D + K) - 2K \} \frac{H}{2\lambda}. \end{aligned}$$

In the following introduction, we use f instead of h and b for simplicity.

2.3. Finite volume method

We define a discretization of the whole physical domain Ω with small cells Ω_i

$$\Omega = \cup \Omega_i, \Omega_i \cap \Omega_j = \emptyset (i \neq j).$$

The whole velocity space is discretized by velocity space cell $\delta \mathbf{u}_k$. The integration of a value Q over the whole velocity space can be expressed as

$$\int Q \, d\mathbf{u} = \sum_k Q_k \mathcal{V}_k,$$

where Q_k is the average of Q over velocity space cell $\delta \mathbf{u}_k$ and $\mathcal{V}_k = \int_{\delta \mathbf{u}_k} d\mathbf{u}$ is the volume of velocity space cell $\delta \mathbf{u}_k$.

By taking the integration of Eq.(1) or Eq.(2) over velocity space cell $\delta \mathbf{u}_k$, we can get the governing equation of distribution function at discretized velocity points

$$\frac{\partial f_k}{\partial t} + \mathbf{u}_k \cdot \nabla f_k = \frac{f_k^+ - f_k}{\tau}, \quad (3)$$

where $f_k = f_k(\mathbf{x}, t) = f(\mathbf{x}, t, \mathbf{u}_k)$. By take integration of above equation over physical cell Ω_i and from time t^n to t^{n+1} , we can get

$$f_{i,k}^{n+1} = f_{i,k}^n - \frac{1}{|\Omega_i|} \sum_{j \in N(i)} S_{ij} \mathcal{F}_{ij,k} + \int_{t^n}^{t^{n+1}} \frac{f_{i,k}^+ - f_{i,k}}{\tau_i} dt,$$

where $f_{i,k}^n$ and $f_{i,k}^{n+1}$ are the average of distribution function over cell Ω_i and $\delta \mathbf{u}_k$ at time t^n and t^{n+1} , $|\Omega_i|$ denotes the volume of cell i , $N(i)$ is the set of all interface-adjacent neighboring cells of cell i and j is one of the neighboring cells of i . The interface between cell i and j is labeled as ij , having an area of S_{ij} . And the microscopic flux $\mathcal{F}_{ij,k}$ is

$$\mathcal{F}_{ij,k} = u_{k,n} \int_{t^n}^{t^{n+1}} f_{ij,k} dt, \quad (4)$$

where $u_{k,n} = \mathbf{u}_k \cdot \mathbf{n}_{ij}$ is the normal velocity via surface ij with normal direction \mathbf{n}_{ij} , and $f_{ij,k}$ is the average distribution function over cell $\delta \mathbf{u}_k$ at the center of cell interface ij .

By taking moments of the above equation and considering the compatibility condition, we can get the governing equation of macroscopic conservative values

$$\mathbf{W}_i^{n+1} = \mathbf{W}_i^n - \frac{1}{\Omega_i} \sum_{j \in N(i)} S_{ij} \mathbf{F}_{ij}, \quad (5)$$

where \mathbf{W}_i^n and \mathbf{W}_i^{n+1} are cell-averaged conservative value at time t^n and t^{n+1} , and the

macroscopic flux is defined by

$$\mathbf{F}_{ij} = \sum_k \mathcal{V}_k \begin{pmatrix} \mathcal{H}_{ij,k} \\ \mathbf{u}_k \mathcal{H}_{ij,k} \\ \frac{1}{2}(\mathbf{u}_k^2 \mathcal{H}_{ij,k} + \mathcal{B}_{ij,k}) \end{pmatrix}, \quad (6)$$

where the $\mathcal{H}_{ij,k}$ and $\mathcal{B}_{ij,k}$ is defined by

$$\begin{aligned} \mathcal{H}_{ij,k} &= u_{k,n} \int_{t^n}^{t^{n+1}} h_{ij,k} \, dt, \\ \mathcal{B}_{ij,k} &= u_{k,n} \int_{t^n}^{t^{n+1}} b_{ij,k} \, dt. \end{aligned}$$

2.4. Gas evolution model

Along the characteristic line, the integral solution of BGK equation (3) gives

$$f_k(\mathbf{r}, t, \boldsymbol{\xi}) = \frac{1}{\tau} \int_{t_0}^t f_k^+(\mathbf{r}', t') e^{-(t-t')/\tau} \, dt' + e^{-t/\tau} f_{0,k}(\mathbf{r} - \mathbf{u}_k t),$$

where $f_{0,k}(\mathbf{r})$ is the initial distribution function at the beginning of each step t_n , and $f^+(\mathbf{r}, t)$ is the effective equilibrium state distributed in space and time around \mathbf{r} and t . The integral solution gives a multiscale modeling of evolution processes from an initial non-equilibrium distribution f to an equilibrium distribution f^+ by collision.

To achieve second-order accuracy, the initial distribution function $f_{0,k}(\mathbf{r})$ is approximated as

$$f_{0,k}(\mathbf{r}) = \begin{cases} f_k^l + \mathbf{r} \cdot \nabla f_k^l, & u_{k,n} > 0, \\ f_k^r + \mathbf{r} \cdot \nabla f_k^r, & u_{k,n} < 0, \end{cases}$$

where f_k^l and f_k^r are the reconstructed initial distribution functions at the left and right sides of the interface. The equilibrium state is approximated as

$$f_k^+(\mathbf{r}, t) \approx g_{0,k} + g_{0,k}^+ + \mathbf{r} \cdot \nabla g_{0,k} + \frac{\partial g_{0,k}}{\partial t} t.$$

g_0 is the Maxwellian distribution function derived from the conservative variables contributed by all particles transported from both sides of the interface. Details of the distribution functions and derivatives are demonstrated in earlier work [64, 14].

In summary, the distribution function at the cell interface is

$$f_k(\mathbf{0}, t, \boldsymbol{\xi}) = \begin{cases} c_1 f_k^l + c_2 \mathbf{u}_k \cdot \nabla f_k^l + c_3 (g_{0,k} + g_{0,k}^+) + c_4 \mathbf{u}_k \cdot \nabla g_{0,k} + c_5 \partial_t \partial g_{0,k}, & u_{k,n} > 0, \\ c_1 f_k^r + c_2 \mathbf{u}_k \cdot \nabla f_k^r + c_3 (g_{0,k} + g_{0,k}^+) + c_4 \mathbf{u}_k \cdot \nabla g_{0,k} + c_5 \partial_t \partial g_{0,k}, & u_{k,n} < 0, \end{cases} \quad (7)$$

and

$$\begin{aligned}
c_1 &= e^{-t/\tau}, \\
c_2 &= -te^{-t/\tau}, \\
c_3 &= 1 - e^{-t/\tau}, \\
c_4 &= te^{-t/\tau} - \tau(1 - e^{-t/\tau}), \\
c_5 &= t - \tau(1 - e^{-t/\tau}).
\end{aligned}$$

2.5. Boundary condition

This paper adopts ghost cells to construct the boundary fluxes. Two types of boundary conditions are considered. This first type is artificially defined boundaries, such as inlets, outlets, and far fields. The conservation variables at the ghost cells are treated with the same boundary conditions as Euler equations, where the distribution function is set to Maxwellian distribution corresponding to the conservative variables. When calculating the fluxes, the distribution functions at cell interfaces are selected based on the velocity direction.

The second type is real wall boundaries, which are treated with the Maxwellian isothermal boundary conditions. The microscopic distribution function at the wall is defined as

$$f_{w,k} = \begin{cases} f_{in,k} + \mathbf{u}_k \cdot \nabla f_{in,k}t, & u_{k,n} > 0 \\ g_w, & u_{k,n} < 0 \end{cases},$$

where $u_{k,n} = \mathbf{u}_k \cdot \mathbf{n}_w$ is the projection of micro velocity on wall-normal direction \mathbf{n}_w , the $f_{in,k}$ and $\nabla f_{in,k}$ is obtained by one-sided interpolation from the interior region, and g_w is defined as

$$g_w = \rho_w \left(\frac{m}{2\pi k T_w} \right) e^{-\frac{m((\mathbf{u}-\mathbf{U}_w)^2 + \xi^2)}{2kT_w}},$$

where T_w and \mathbf{U}_w is given wall temperature and velocity, and ρ_w is calculated by

$$\sum_k \mathcal{V}_k u_{k,n} \int_{t^n}^{t^{n+1}} h_{w,k} dt = 0, \tag{8}$$

which means no particle penetrating the wall.

Then, we can obtain the flux of the microscopic distribution function

$$\mathcal{F}_{w,k} = \begin{cases} u_{k,n}(f_{in,k} + \mathbf{u}_k \cdot \nabla f_{in,k}t), & u_{k,n} > 0 \\ u_{k,n}g_w, & u_{k,n} < 0 \end{cases},$$

and the macroscopic flux $\mathbf{F}_w = (F_{w0}, F_{w1}, F_{w2}, F_{w3}, F_{w4})^T$ can be obtained through Eq.(6). And by denoting the surface flux of momentum equation as $\mathbf{F}_{mw} = (F_{w1}, F_{w2}, F_{w3})$, we can obtain surface pressure

$$p_w = \mathbf{F}_{mw} \cdot \mathbf{n}_w,$$

the shear stress

$$\sigma_w = |\mathbf{F}_{mw} - p_w \mathbf{n}_w|,$$

and the heat flux

$$q_w = F_{w4}.$$

2.6. Source term

The source term can be discretized by the trapezoidal rule,

$$\int_{t^n}^{t^{n+1}} \frac{f_{i,k}^+ - f_{i,k}}{\tau_i} dt = \frac{\Delta t}{2} \left(\frac{f_{i,k}^{+(n+1)} - f_{i,k}^{n+1}}{\tau_i^{n+1}} + \frac{f_{i,k}^{+(n)} - f_{i,k}^n}{\tau_i^n} \right),$$

where the $f^{+(n+1)}$ and τ^{n+1} can be obtained through the macroscopic conservative values \mathbf{W}^{n+1} . Considering the microscopic govern equation, the distribution function can be updated by

$$f_{i,k}^{n+1} = \left(1 + \frac{\Delta t}{2\tau_i^{n+1}} \right)^{-1} \left[f_{i,k}^n - \frac{1}{\Omega_i} \sum_{j \in N(i)} S_{ij} \mathcal{F}_{ij,k} + \frac{\Delta t}{2} \left(\frac{f_{i,k}^{+(n+1)}}{\tau_i^{n+1}} + \frac{f_{i,k}^{+(n)} - f_{i,k}^n}{\tau_i^n} \right) \right]. \quad (9)$$

3. Algorithm

3.1. Basic UGKS algorithm

The algorithm of the UGKS is summarized as follows:

- Step 1** Calculate time step and heat flux.
- Step 2** Reconstruction. The constraint least-square reconstruction and gradients compressor factors [65] are used to get the gradients of macroscopic values, and the constraint least-square reconstruction and Venkatakrishnan limiter are used to get the gradients of microscopic values.
- Step 3** Evaluate flux. Calculate the microscopic flux by Eq.(4) and Eq.(7), and get the corresponding macroscopic flux through Eq.(6).
- Step 4** Update flow fields. Apply Eq.(5) to obtain the macroscopic quantities of the full field at the $n + 1$ step. Then calculate Eq.(9) to update the microscopic distribution function.

3.2. Two stage update of microscopic distribution function

Due to the original algorithm, we need to store all the gradients and spatial residuals of the distribution functions, which requires a significant amount of memory because of the large number of velocity space meshes. To address this, we can consider updating the distribution functions one by one, thus eliminating the need to store the gradients of all distribution functions.

However, according to Eq.(9), the update of the microscopic distribution functions requires the macroscopic values at time t^{n+1} through $f^{+(n+1)}$. Therefore, we must store the spatial residuals and distribution functions at time t^n to perform the updates. We propose splitting the update process into two steps. The first step is given by

$$\tilde{f}_{i,k}^{n+1} = f_{i,k}^n - \frac{1}{\Omega_i} \sum_{j \in N(i)} S_{ij} \mathcal{F}_{ij,k} + \frac{\Delta t}{2} \frac{f_{i,k}^{+(n)} - f_{i,k}^n}{\tau_i^n}. \quad (10)$$

The second step is defined as

$$f_{i,k}^{n+1} = \left(1 + \frac{\Delta t}{2\tau_i^{n+1}}\right)^{-1} \left(\tilde{f}_{i,k}^{n+1} + \frac{\Delta t}{2} \frac{f_{i,k}^{+(n+1)}}{\tau_i^{n+1}}\right). \quad (11)$$

In this approach, we can update the distribution function one by one in velocity space using Eq.(10), which only requires storing the gradients and residuals for one distribution function. Furthermore, after obtaining $\tilde{f}_{i,k}^{n+1}$, the variable $f_{i,k}^n$ is no longer needed, allowing us to reuse the same block of memory to store $\tilde{f}_{i,k}^{n+1}$.

Additionally, several terms need further clarification.

- In the calculation of the Shakhov model, the heat flux is needed, which needs the momentum of distribution at the cell interface. However, we use the averaged heat flux of left and right cells for simplicity.
- In the calculation of microscopic flux, the equilibrium part and time coefficients only depend on macroscopic values, so we can calculate it first and store it at the cell interface.
- As shown in Eq.(8), the Maxwellian wall boundary condition needs the whole velocity space values to get density, so we need to store the distribution functions at the wall and evolve flux individually.

As a result, the UGKS algorithm has been shown in Algorithm 1.

3.3. Parallelization of the UGKS

In this section, we present the parallelization of our code based on the Message Passing Interface (MPI). First, we need to identify the messages that must be exchanged:

- The macroscopic reconstruction requires the macroscopic values of adjacent cells.
- The calculation of the equilibrium state and time coefficients necessitates the macroscopic values, their gradients, and the heat flux of adjacent cells.
- The microscopic reconstruction requires the microscopic distribution functions of adjacent cells.

Algorithm 1 Algorithm for Time Step Calculation and Flux Evolution

- 1: Calculate the time step Δt based on the CFL condition and compute heat flux for each cell.
 - 2: Reconstruct the macroscopic values.
 - 3: Calculate the equilibrium state and time coefficients for cell interfaces.
 - 4: **for** $k = 1$ to k_{\max} **do**
 - 5: Reconstruct the microscopic values for f_k .
 - 6: Evolve the flux \mathcal{F}_k using Eq.(4) and calculate their contribution to the macroscopic flux using Eq.(6).
 - 7: Interpolate f_k and their gradients at the boundary.
 - 8: Update f_k^n to \tilde{f}_k^{n+1} using Eq.(10).
 - 9: **end for**
 - 10: Evolve the flux at the boundary.
 - 11: Update macroscopic values using Eq.(5).
 - 12: Update microscopic values using Eq.(11).
-

- The flux evolution requires the microscopic distribution functions and their gradients of adjacent cells.

Compared with the macroscopic values, the microscopic values need more times of exchanges because of the huge number of velocity space mesh cells. The evolution of the microscopic distribution function from f_k^n to \tilde{f}_k^{n+1} is illustrated in Figure 1. It is important

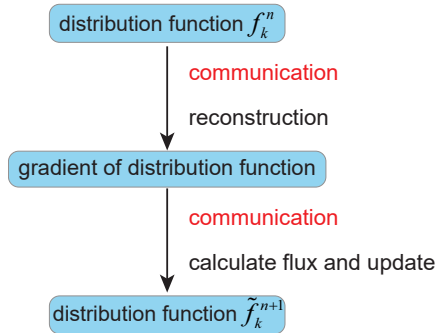


Figure 1: The update of the microscopic distribution function f_k^n to \tilde{f}_k^{n+1} .

to note that we need to perform two message exchanges at each microscopic speed point. We must first exchange the microscopic distribution functions and then exchange their gradients, as the gradients depend on the microscopic distribution functions. However, the microscopic distribution functions at different microscopic velocity points are independent. Therefore, we can combine the two communications by reconstructing and evolving different velocity points within the same loop. As shown in Figure 2, we perform the evolution of f_k and the reconstruction of f_{k+1} within a single loop.

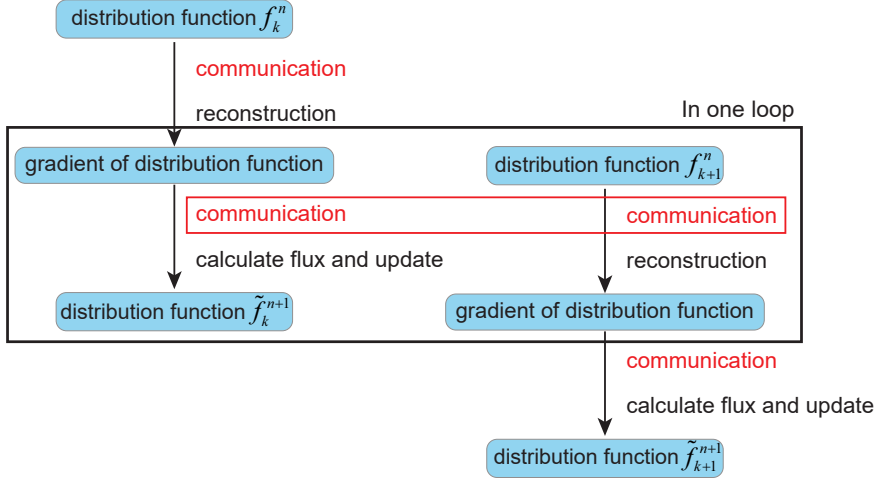


Figure 2: Combining communications by reconstructing and evolving different velocity points within the same loop.

Next, we consider memory usage. The entire space of the distribution function must be stored. However, the gradient of the distribution function does not need to be stored once the spatial residuals are obtained. In the new algorithm designed for MPI communication, we require two blocks of memory to store the gradients. As illustrated in Figure 3, we only need to store two gradients for each loop. For example, in loop k , we only need to store

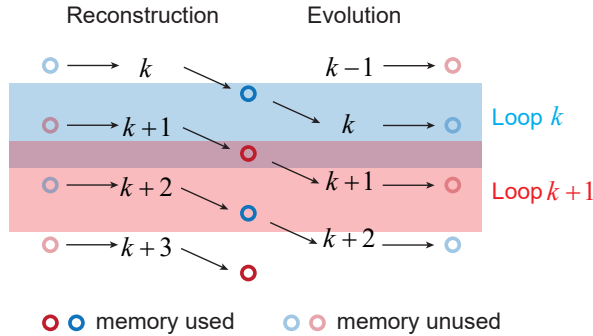


Figure 3: Memory usage for the distribution function gradient.

the gradients ∇f_k^n and ∇f_{k+1}^n . In the subsequent loop $k+1$, the gradient ∇f_k^n is no longer needed, allowing that block of memory to be repurposed for storing ∇f_{k+2}^n .

In summary, we illustrate the calculation processes, message communication, and memory usage in Figure 4. Non-blocking communication is also used in this process. Considering other parts of the algorithm, the whole parallelized algorithm is shown as Algorithm 2.

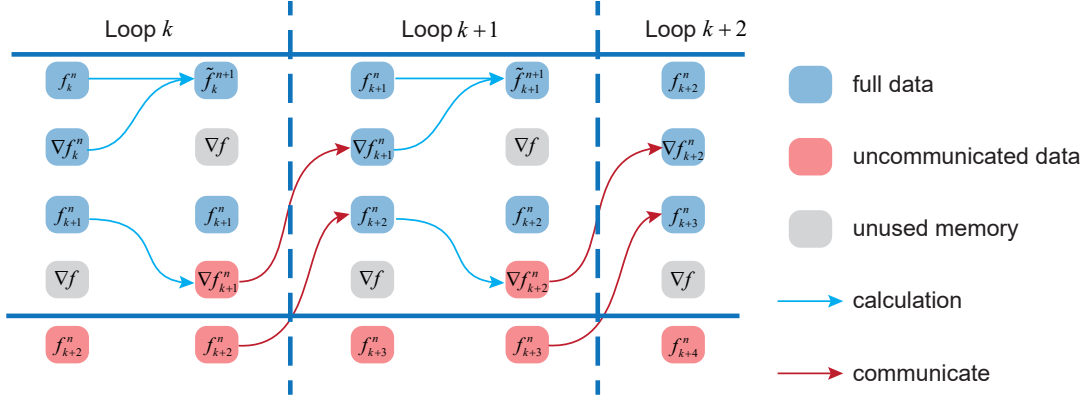


Figure 4: The summary of the calculation processes, message communication and memory usage of the updation from f_k^n to f_k^{n+1} .

4. Numerical example

4.1. Hypersonic flow around a circular cylinder

Hypersonic gas flow of argon with Prandtl number $Pr = 2/3$ around a circular cylinder has been simulated at $Ma_\infty = 5$ and $Kn_\infty = 0.1$. The characteristic length used to define the Knudsen number is the cylinder diameter $D = 2$ m. The temperature of free stream flow is $T_\infty = 273$ K, and an isothermal wall with a fixed temperature of $T_w = 273$ K is applied for the cylinder surface. The physical domain is discretized by 12,600 (180×70) quadrilateral cells with the height of first layer mesh $h = 0.001$ m, while the unstructured discrete velocity space (DVS) mesh consists of 2,060 cells as shown in Figure 5. The DVS is discretized in a circle region with the center $0.4 \times (U_\infty, 0)$ with a total radius of $6\sqrt{RT_s}$ where T_s is the stagnation temperature of the free stream flow. The unstructured DVS mesh is refined at zero velocity point with a radius of $3\sqrt{RT_w}$ and the free stream point with a radius of $3\sqrt{RT_\infty}$.

The contours of Mach number and temperature are plotted in Figure 6. To verify the result quantitatively, the non-dimensionalized surface coefficients (the pressure coefficient C_p , the shear stress coefficient C_t , and the heat flux coefficient C_h) are defined by

$$C_p = \frac{p_s}{\frac{1}{2}\rho_\infty U_\infty^2}, C_t = \frac{f_s}{\frac{1}{2}\rho_\infty U_\infty^2}, C_h = \frac{h_s}{\frac{1}{2}\rho_\infty U_\infty^3},$$

where U_∞ is the incoming flow speed calculated by free-stream Mach number Ma_∞ , p_s is the surface pressure, f_s is the surface friction and h_s is the surface heat flux. As shown in Figure 7, our results agree well with the results of the DSMC method [46].

To further verify the computational accuracy and robustness of the current scheme, hypersonic flow passing over a circular cylinder at a huge Mach number $Ma_\infty = 15$ and $Kn_\infty = 0.01$ is simulated. The characteristic length used to define the Knudsen number is the cylinder diameter $D = 1$ m. The temperature of free stream flow is $T_\infty = 273$ K, and an isothermal wall with a fixed temperature of $T_w = 273$ K is applied for the cylinder

Algorithm 2 Parallel Algorithm for the UGKS

- 1: Calculate the time step Δt based on the CFL condition and compute heat flux for each cell.
 - 2: **Send macroscopic values, heat flux, and microscopic distribution function f_1 .**
 - 3: **Receive macroscopic values, heat flux, and microscopic distribution function f_1 .**
 - 4: Reconstruct macroscopic values.
 - 5: Reconstruct microscopic values for f_1 and store their gradients as ∇f_1 .
 - 6: **Send gradients of macroscopic values, microscopic distribution function f_2 , and gradients of microscopic values ∇f_1 .**
 - 7: **for** $k = 1$ to k_{\max} **do**
 - 8: Let $\&\nabla f_f \leftarrow (k \bmod 2 == 1) ? \nabla f_1 : \nabla f_2$ and $\&\nabla f_r \leftarrow (k \bmod 2 == 1) ? \nabla f_2 : \nabla f_1$.
 - 9: **if** $k == 1$ **then**
 - 10: **Receive gradients of macroscopic values, distribution function f_2 , and gradients of microscopic ∇f_f .**
 - 11: Calculate equilibrium state and time coefficients for cell interfaces.
 - 12: **else**
 - 13: **Receive distribution function f_{k+1} and gradients of microscopic ∇f_f .**
 - 14: **end if**
 - 15: Reconstruct microscopic values for f_{k+1} and store their gradients as ∇f_r .
 - 16: **Send microscopic distribution function f_{k+2} and gradients of microscopic values ∇f_r .**
 - 17: Evolve flux \mathcal{F}_k with f_k and ∇f_f using Eq.(4), and their contribution to macroscopic flux using Eq.(6).
 - 18: Interpolate f_k and their gradients into the boundary.
 - 19: Update f_k^n to \tilde{f}_k^{n+1} using Eq.(10).
 - 20: **end for**
 - 21: Evolve flux at the boundary.
 - 22: Update macroscopic values using Eq.(5).
 - 23: Update microscopic values using Eq.(11).
-

surface. The physical domain is discretized by 14,000 (200×70) quadrilateral cells with the height of first layer mesh $h = 1 \times 10^{-4}$ m, while the unstructured discrete velocity space (DVS) mesh consists of 3,420 cells, as shown in Figure 8. The DVS is discretized in a circle region with the center $0.4 \times (U_\infty, 0)$ with a total radius of $5\sqrt{RT_s}$ where T_s is the stagnation temperature of the free stream flow. The unstructured DVS mesh is refined at zero velocity point with a radius of $5\sqrt{RT_w}$ and the free stream point with a radius of $5\sqrt{RT_\infty}$.

The contours of Mach number and temperature of hypersonic flow at $\text{Kn} = 0.01$ and $\text{Ma} = 15$ passing over a circular cylinder are shown in Figure 9. To further verify our code, the surface quantities compared with the DSMC method [46] are shown in Figure 10.

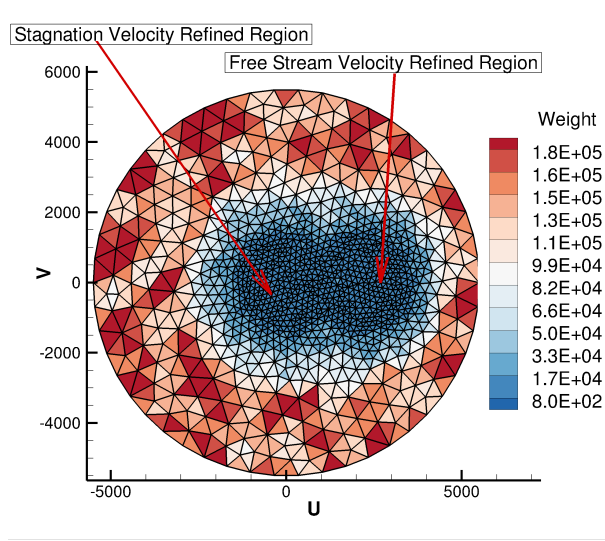


Figure 5: Unstructured DVS mesh with 2,060 cells used for hypersonic flow at $\text{Kn}_\infty = 0.1$ and $\text{Ma}_\infty = 5$ passing over a cylinder by the current UGKS program.

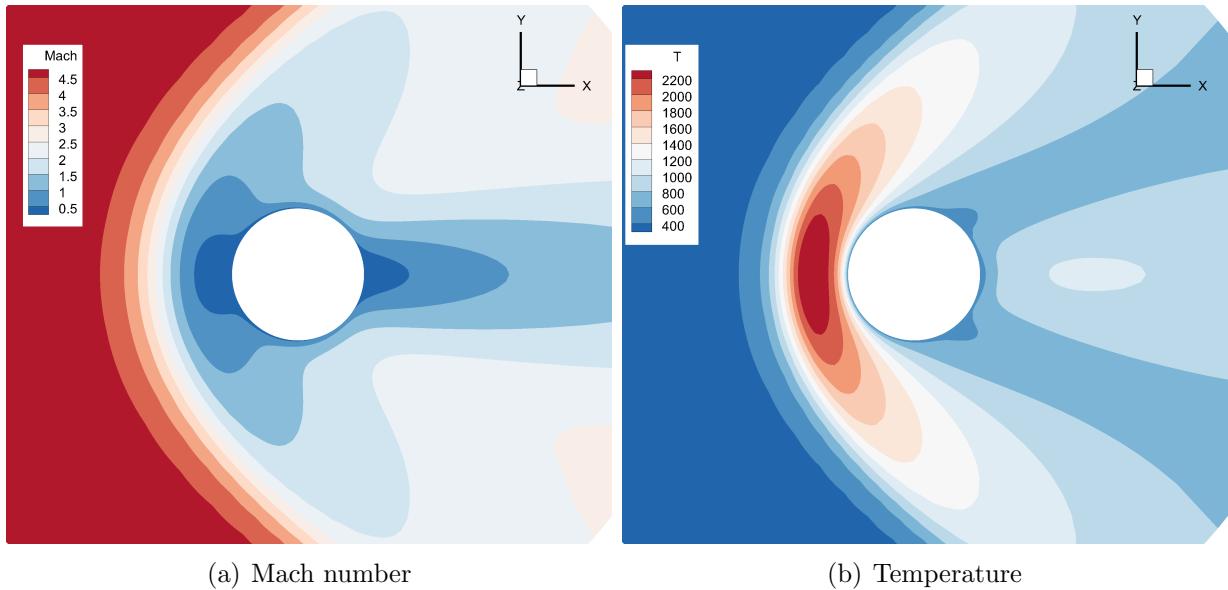


Figure 6: Contours of hypersonic flow at $\text{Kn}_\infty = 0.1$ and $\text{Ma}_\infty = 5$ passing over a circular cylinder by the current UGKS program.

4.2. Supersonic flow around a sphere

To verify further our code in three-dimensional supersonic flow, the supersonic flow passing over a sphere at Mach number 4.25 for $\text{Kn}_\infty = 0.031$ and $\text{Kn}_\infty = 0.121$ are simulated for argon gas with Prandtl number $\text{Pr} = 0.72$. The characteristic length is the sphere diameter $D = 2$ m to define the Knudsen number. The physical domain contains $3,082 \times 37$ hexahedron cells. The physical domain mesh and sphere surface mesh are shown in Figure

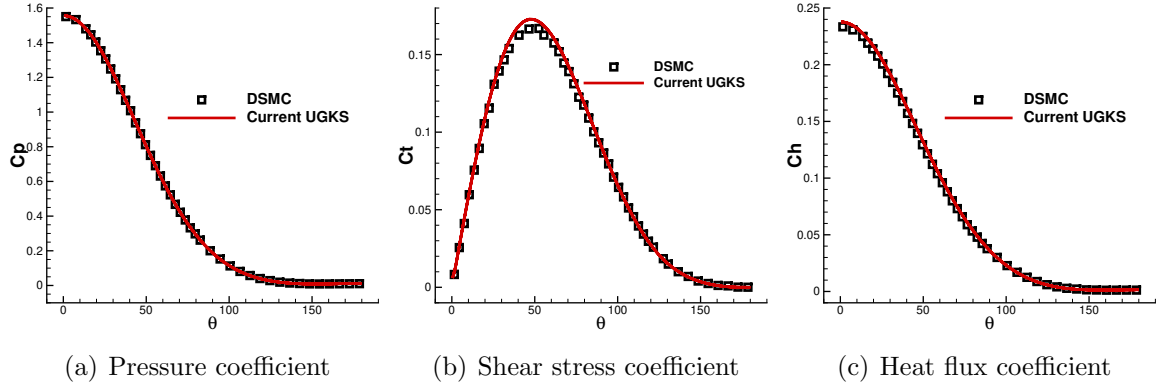


Figure 7: Surface quantities of hypersonic flow at $Kn_\infty = 0.1$ and $Ma_\infty = 5$ passing over a circular cylinder by the current UGKS program compared with the DSMC method [46].

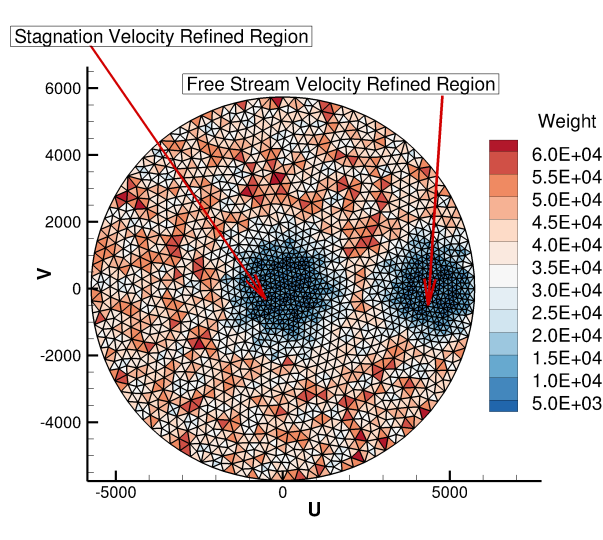


Figure 8: Unstructured DVS mesh with 3,420 cells used for hypersonic flow at $Kn_\infty = 0.01$ and $Ma_\infty = 15$ passing over a cylinder by the current UGKS program

11. The height of the first layer mesh is set as 5×10^{-3} m, and the computational domain is set as a spherical domain with the radius $R < 6$ m. Figure 12 illustrates the section view of unstructured DVS mesh with 11,740 cells. The DVS is discretized into a sphere mesh with a radius of $5\sqrt{RT_{\max}}$, where T_{\max} is the maximum temperature estimated by GKS result as the initial field of the UGKS. The sphere center is located at the zero point. The velocity space near the zero and free stream velocity points are refined.

Figures 13 and 14 depict the contour of Mach number and temperature by our code for different Kn_∞ . To further verify the ability to accurately predict surface quantities, the pressure coefficient, shear stress coefficient, and heat flux coefficient are compared with DSMC results [46], shown in Figure 16 and Figure 15. The result of the pressure coefficient, shear stress coefficient, and heat flux coefficient agree well with the DSMC result.

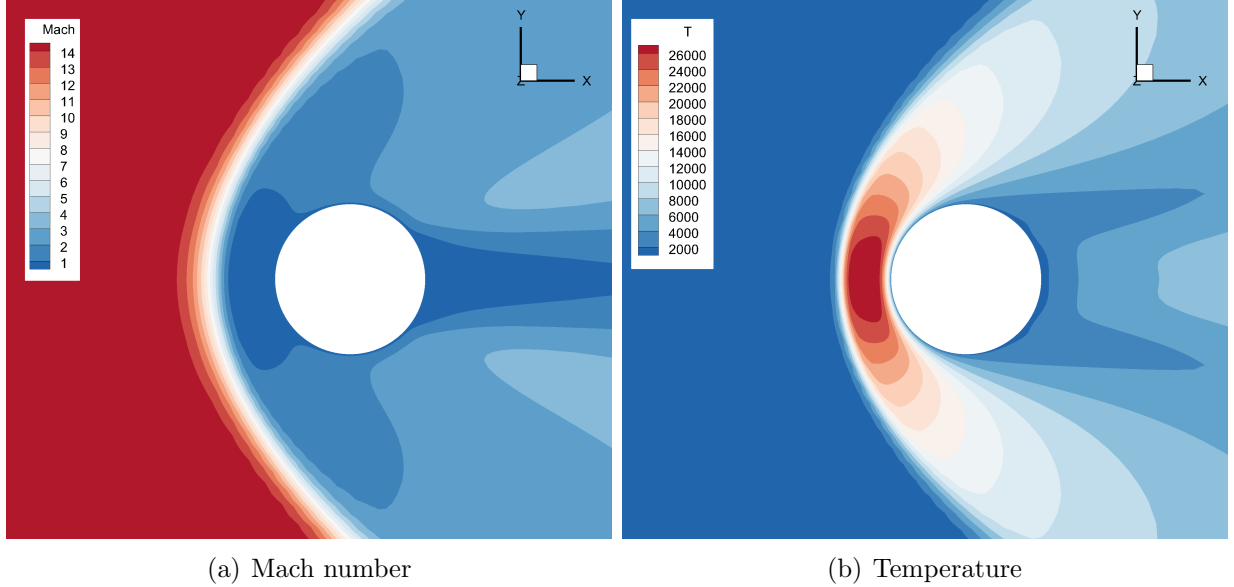


Figure 9: Contours of hypersonic flow at $Kn_\infty = 0.01$ and $Ma_\infty = 15$ passing over a circular cylinder by the current UGKS program.

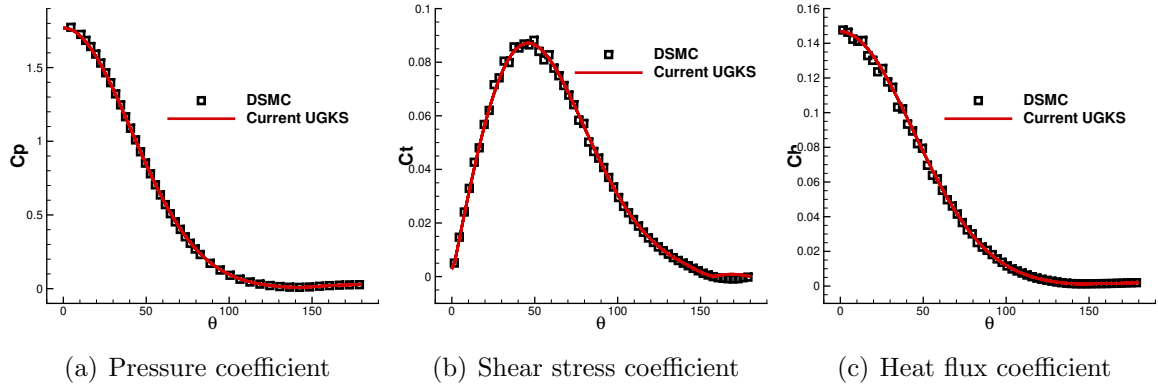


Figure 10: Surface quantities of hypersonic flow at $Kn_\infty = 0.01$ and $Ma_\infty = 15$ passing over a circular cylinder by the current UGKS program compared with the DSMC method [46].

4.3. Lid-driven cavity flow

The three-dimensional lid-driven cavity flows at different Knudsen numbers are used to verify our code. The monatomic gas with the Prandtl number $2/3$ is used in this case. The gas constant is set as $R = 208.14 \text{ J/kg} \cdot \text{K}$ and $\omega = 0.74$. Three Knudsen numbers, 1, 0.1 and 0.01, are tested in this section. The physical domain is $[0, 1]^3$ and discretized with 20^3 hexahedron cells. The wall temperature is 273 K, and the upper wall moves with x -direction velocity of 50.567 m/s. The initial condition is set as a zero-velocity field with a temperature of 273 K. Figure 17 illustrates the section view of unstructured DVS mesh with 17,182 cells. The DVS is discretized into a sphere mesh with a radius of $5\sqrt{RT_w}$, whose center is located at the zero point. The velocity space near the zero point is refined.

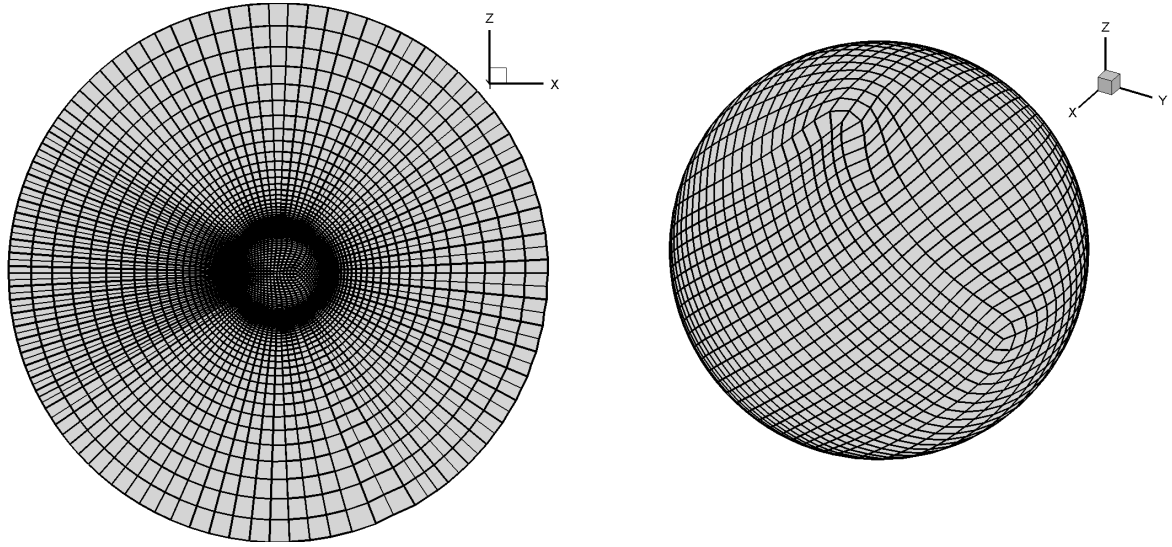


Figure 11: Physical domain mesh used for supersonic flow at $Ma_\infty = 4.25$ passing over spheresphere by the current UGKS program.

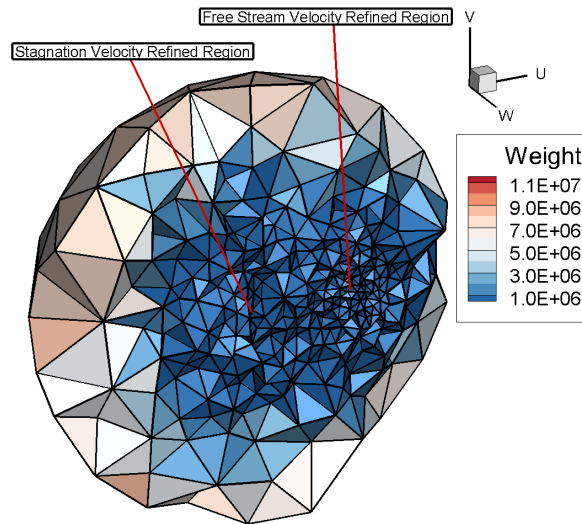


Figure 12: Unstructured DVS mesh consisting of 11,740 cells for supersonic flow at $Ma_\infty = 4.25$ passing over sphere by the current UGKS program.

The computational results are presented in Figures 18, 19, and 20. These figures include the velocity profiles along the central lines, compared with reference data obtained by the discrete velocity method(DVM) [66] and the temperature contours. These results indicate that our scheme can effectively address problems ranging from rarefied flow to near-continuous flow.

We now discuss the parallel efficiency of our code when applied to small-scale problems. The testing platform consists of an AMD Ryzen Threadripper 2990WX CPU operating at

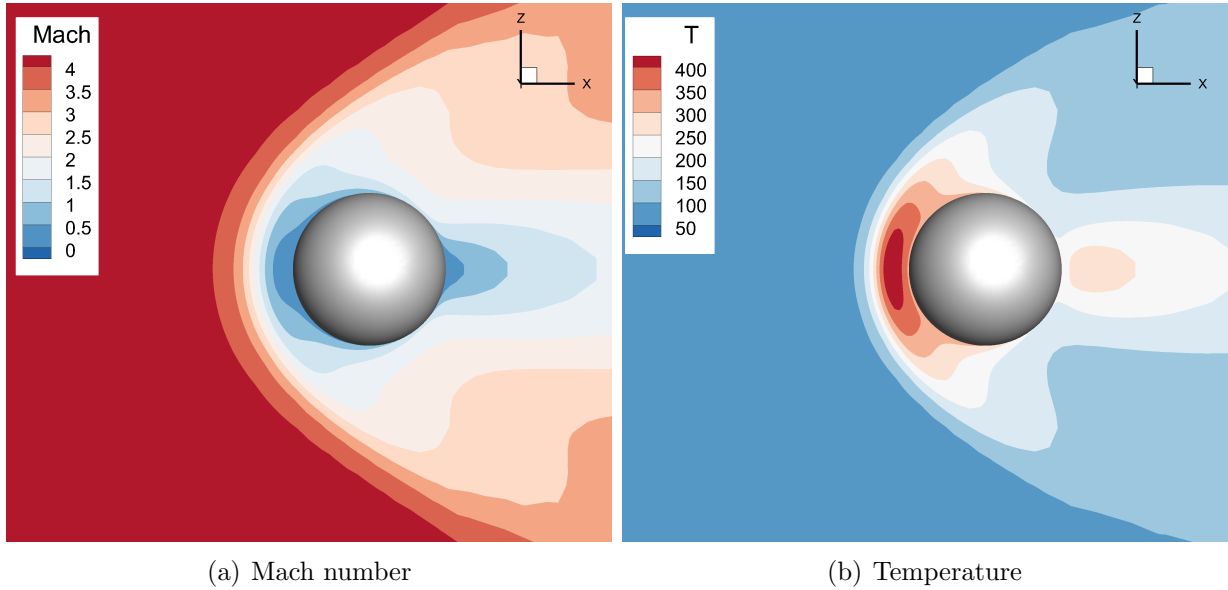


Figure 13: Contours of supersonic flow around a sphere at $Ma_\infty = 4.25$ for $Kn_\infty = 0.031$ by the current UGKS program.

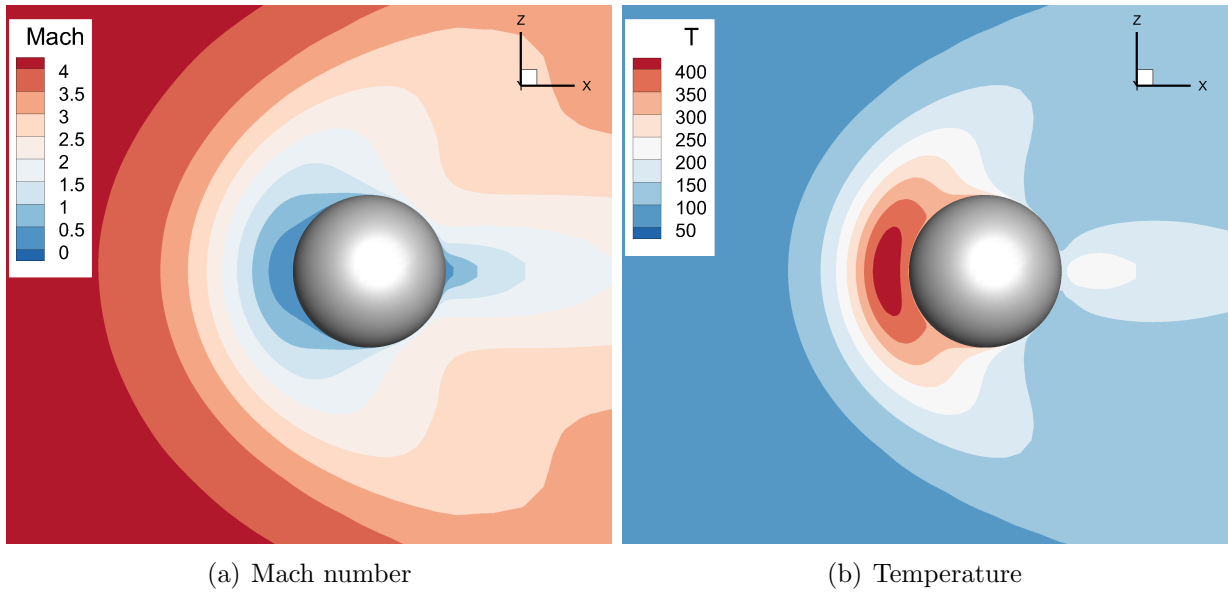


Figure 14: Contours of supersonic flow around a sphere at $Ma_\infty = 4.25$ for $Kn_\infty = 0.121$ by the current UGKS program.

4.2 GHz, featuring 32 cores and 128 GB of memory. The code is compiled using GCC version 11.4.0 with the `-O2` optimization flag and is linked to Open MPI version 4.1.5. We conducted tests using varying cores, ranging from 1 to 32. The computational times for running ten steps and parallel efficiency are presented in Figure 21(a). The results indicate

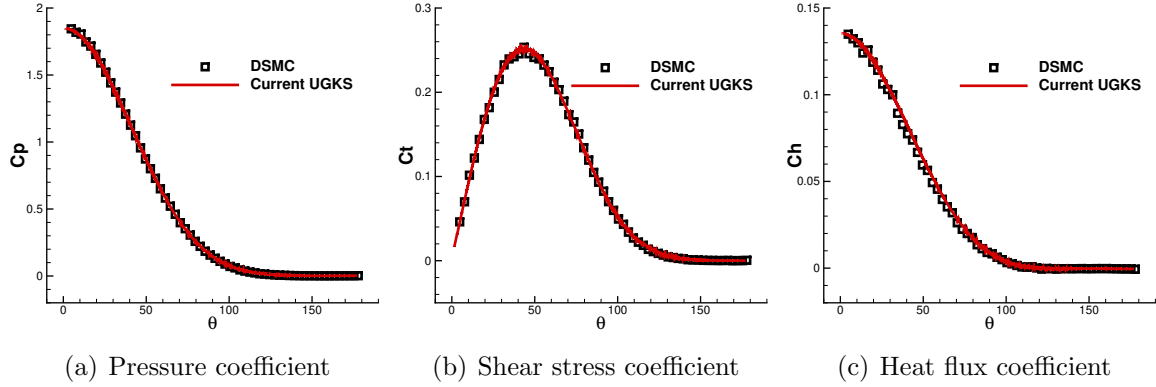


Figure 15: Surface quantities of supersonic flow around a sphere at $Ma_\infty = 4.25$ for $Kn_\infty = 0.031$ by the current UGKS program compared with the DSMC method [46].

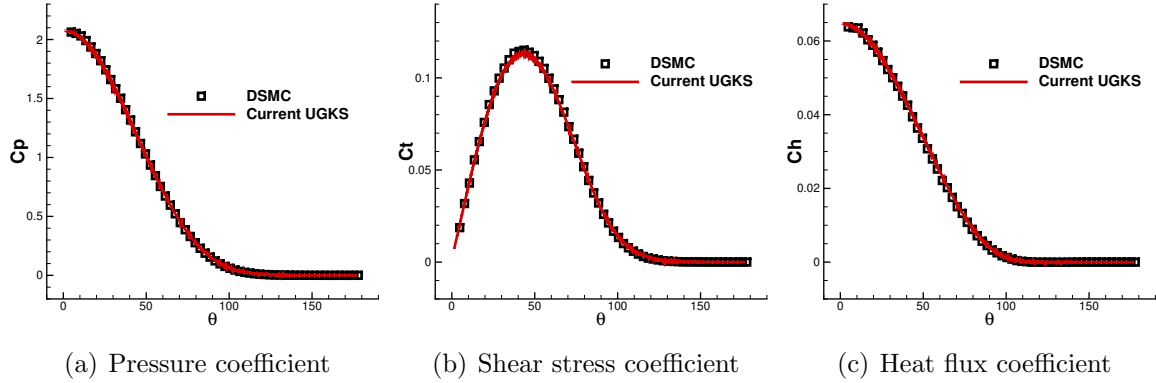


Figure 16: Surface quantities of supersonic flow around a sphere at $Ma_\infty = 4.25$ for $Kn_\infty = 0.121$ by the current UGKS program compared with the DSMC method [46].

that parallel efficiency approaches 100% when utilizing fewer than 16 cores. Additionally, as illustrated in Figure 21(b), both the cache miss ratio and L1 miss ratio are lower when employing 4 and 8 cores, which explains the observed parallel efficiency exceeding 100%.

Next, we discuss memory usage. The memory consumption is approximately 5.3 GB for computations using a single core. We consider a configuration with 8,000 cells and $(6 \times 20 \times 20 = 2,400)$ boundary faces to analyze theoretical memory usage. Each cell at one velocity space point requires two doubles to store the reduced distribution function. We need to store both the distribution functions and their gradients for wall surfaces, necessitating eight doubles for each face at one velocity space point. In total, the memory required to store all distribution functions is given by $(8,000 \times 2 + 2,400 \times 8) \times 17,182$ doubles, which amounts to approximately 4.5 GB. In this case, only 0.8 GB (less than 20% of the theoretical memory) is needed to store other data.

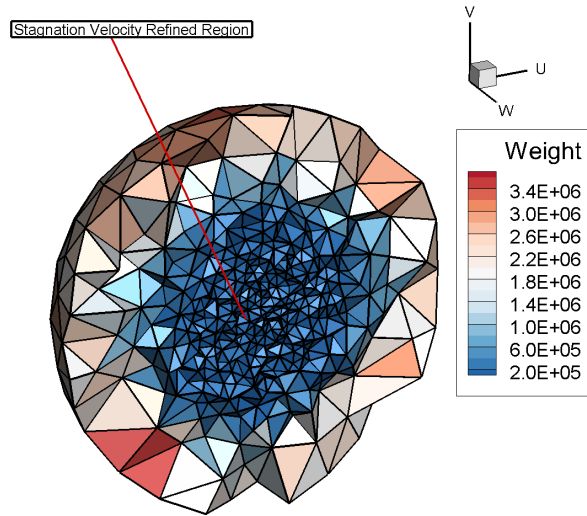
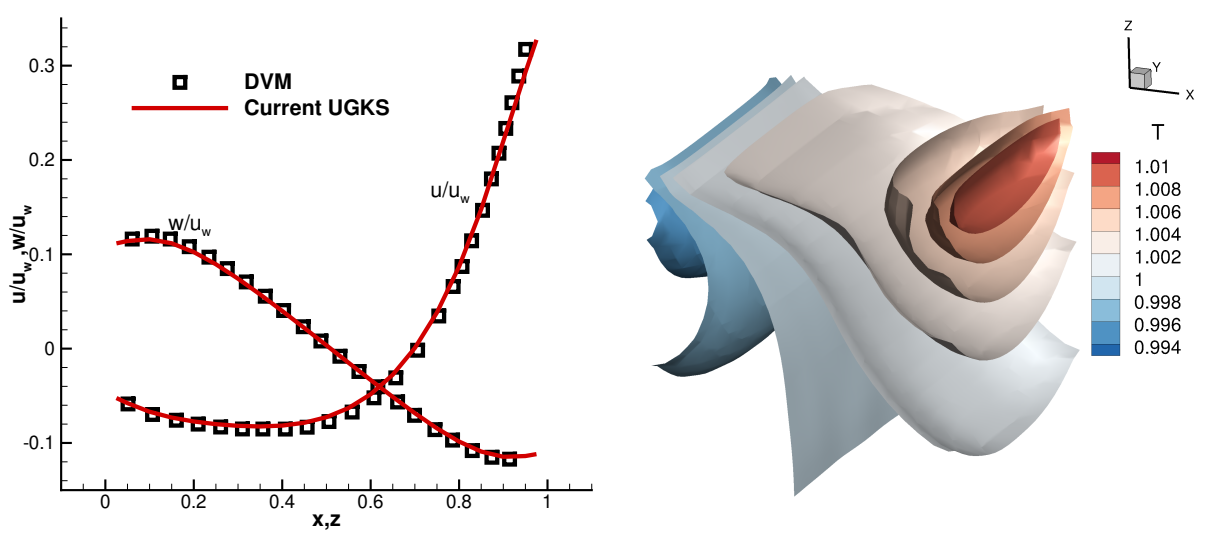


Figure 17: Unstructured DVS mesh used for cavity flow by the current UGKS program.



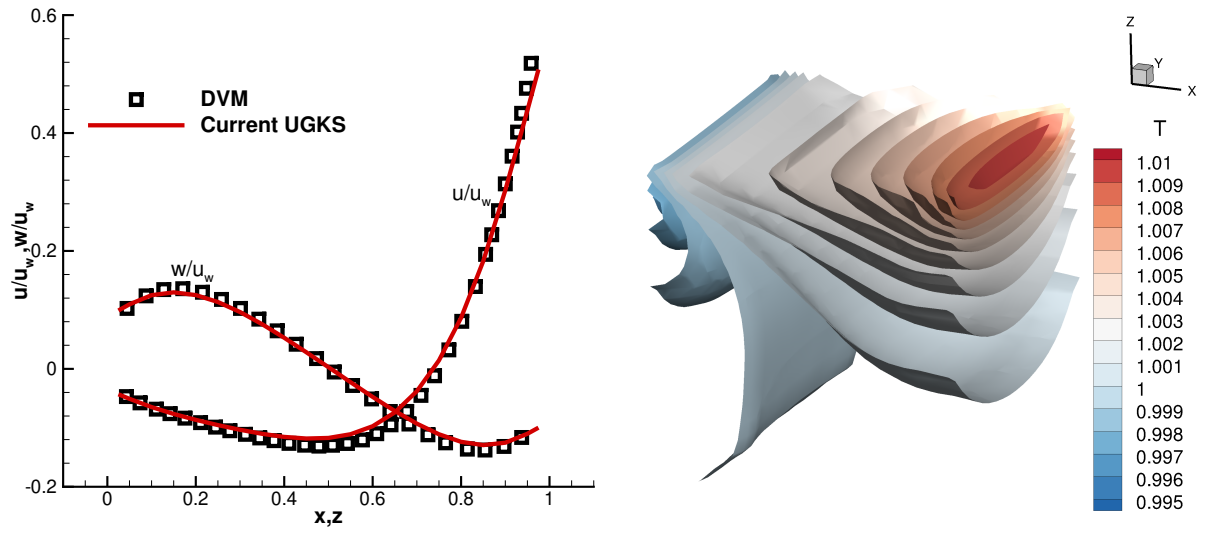
(a) Velocity profiles along the central lines compared with the DVM [66]

(b) Temperature contour

Figure 18: 3D lid-driven cavity flow at $Kn = 1$ by the current UGKS program.

4.4. Hypersonic flow around an X38-like space vehicle

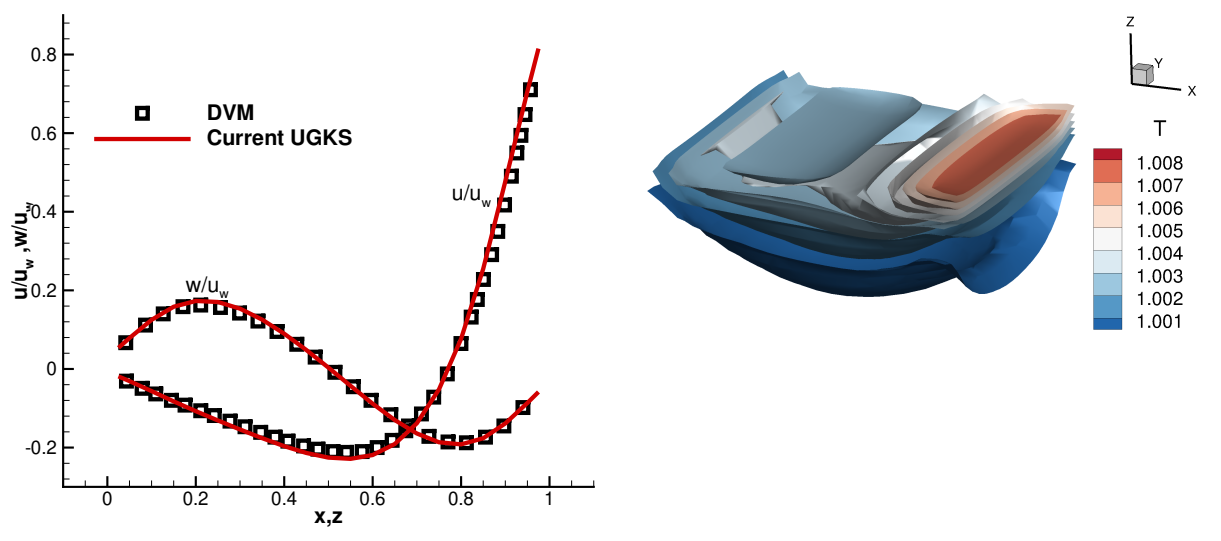
This case is used to study our program's capability to handle a larger number of grids. Hypersonic flow at $Ma_\infty = 8.0$ passing over an X38-like vehicle for $Kn_\infty = 0.00275$ at angles of attack of $AoA = 20^\circ$ is simulated. The reference length to define the Knudsen number is $L_{ref} = 0.28$ m. In this case, all flow regimes are involved due to the hypersonic free stream flow in the transition regime and the complex geometric shape, posing a great challenge to the numerical solver. The free stream temperature is $T_\infty = 56$ K, and an isothermal wall is



(a) Velocity profiles along the central lines compared with the DVM [66]

(b) Temperature contour

Figure 19: 3D lid-driven cavity flow at $Kn = 0.1$ by the current UGKS program.



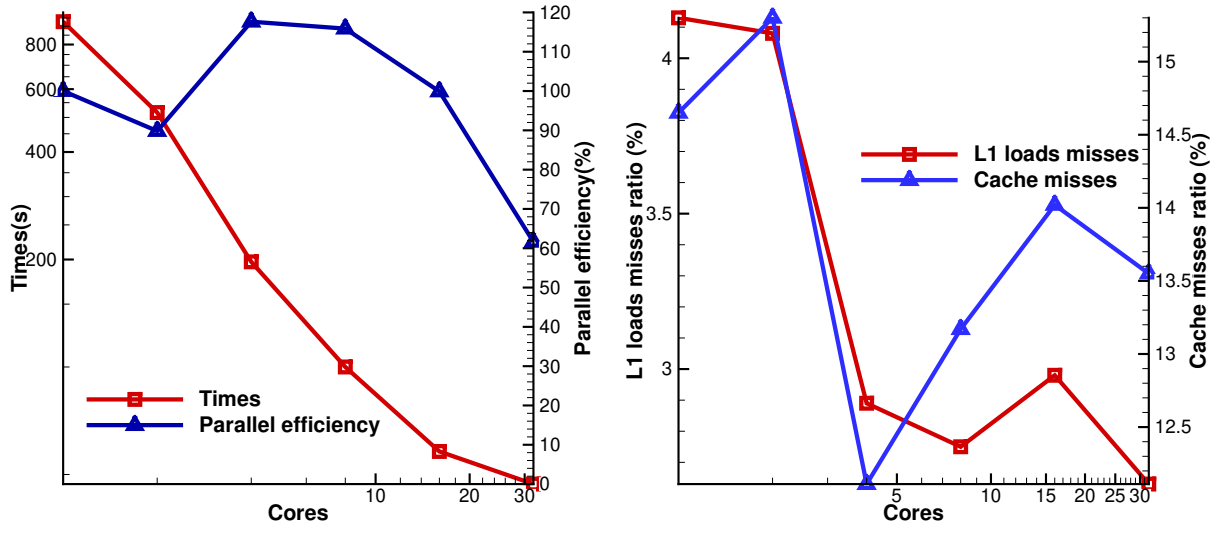
(a) Velocity profiles along the central lines compared with the DVM [66]

(b) Temperature contour

Figure 20: 3D lid-driven cavity flow at $Kn = 0.01$ by the current UGKS program.

applied to the vehicle surface with $T_w = 302$ K.

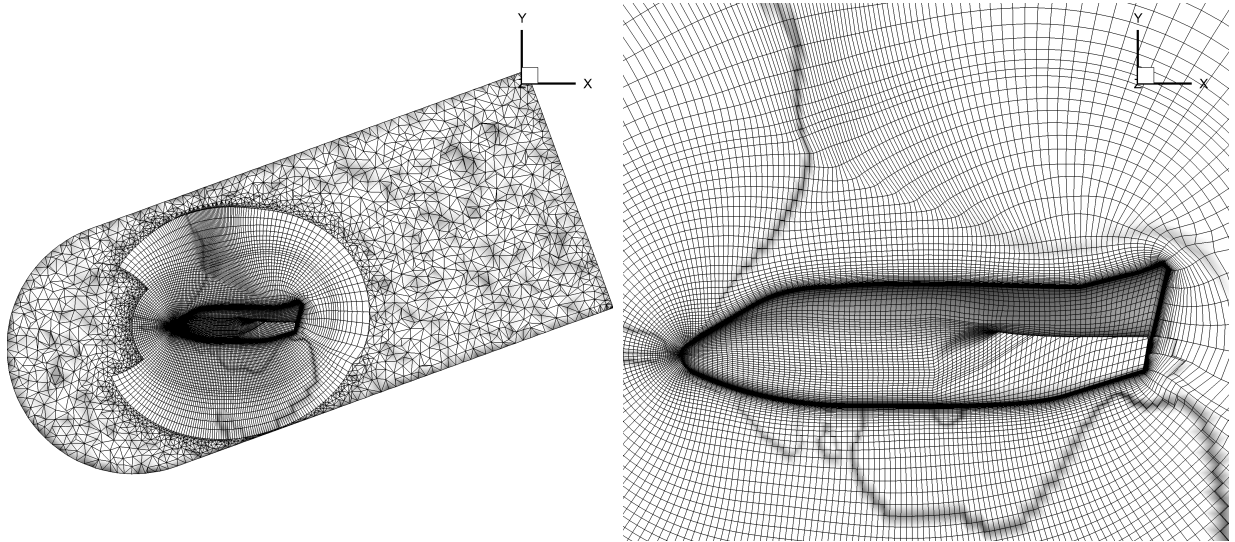
The physical mesh consists of 1,058,685 cells with the cell height of the first layer mesh $h = 1.5 \times 10^{-4}$ m, as shown in Figure 22. The unstructured DVS mesh is depicted in Figure 23. The DVS is discretized into 4,548 cells in a sphere mesh with a radius of $4\sqrt{RT_s}$.



(a) Computational times and parallel efficiency

(b) Cache and L1 misses ratio

Figure 21: Parallel computational performance of cavity by the current UGKS program.



(a) Half of the domain

(b) Close view of the vehicle surface

Figure 22: Section view of the physical mesh of X38-like space vehicle with 600,078 cells by the current UGKS program.

velocity space near the zero and free stream velocity points are refined within a spherical region of radius $r = \sqrt{RT_w}$ and $r = \sqrt{RT_\infty}$ respectively.

The contour of Mach number and temperature are shown in Figure 24. Figure 25 depicts the surface quantities on the symmetric cross-section perpendicular to the y -axis and comparisons with the DSMC data. All the coefficients predicted by our code align well with

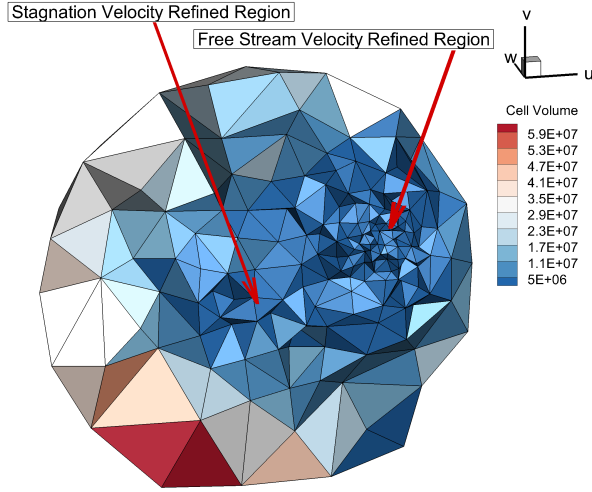


Figure 23: Unstructured DVS mesh with 4,548 cells used for hypersonic flow at $Mach_\infty = 8.0$ and $Kn_\infty = 0.00275$ passing over an X38-like space vehicle by the current UGKS program.

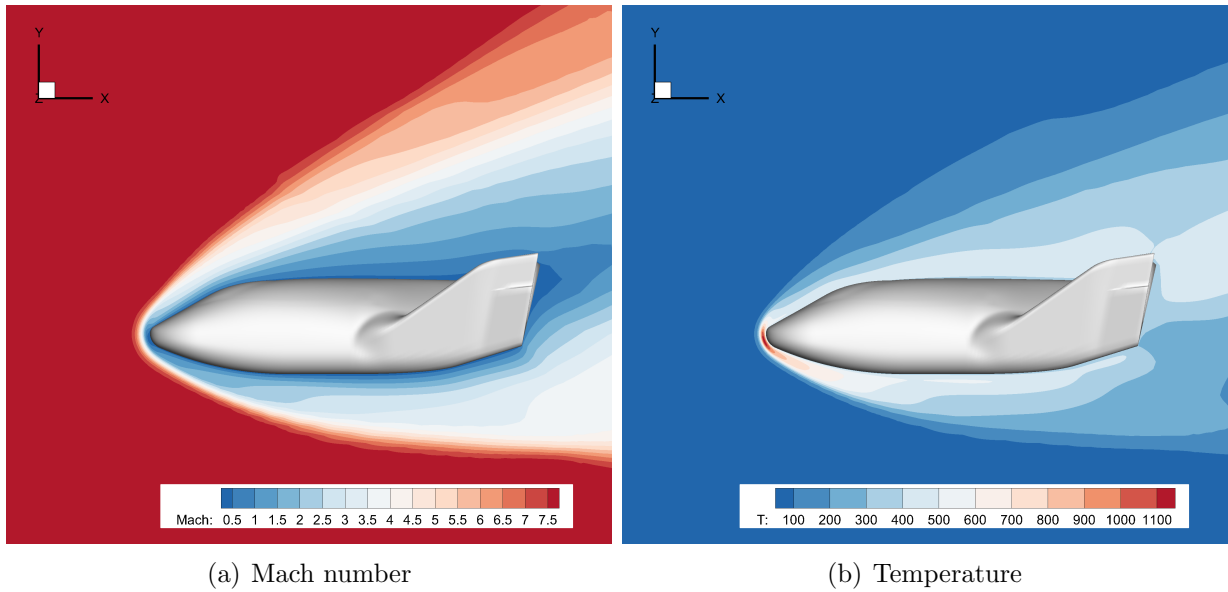


Figure 24: The contour of hypersonic flow around an X38-like space vehicle at $Mach_\infty = 8.0$ and $Kn_\infty = 0.00275$ by the current UGKS program.

the DSMC reference [67].

We now discuss the parallel efficiency of our code on large-scale problems. The simulation is conducted on the SUGON computation platform using a CPU 7285 (32 cores, 2.5GHz). The code is compiled using GCC version 7.3.1 with the `-O2` optimization flag and is linked to Open MPI version 4.1.5. To provide a more intuitive demonstration of the program's parallel efficiency, we first conducted tests using the gas-kinetic scheme (GKS) [68], which has a

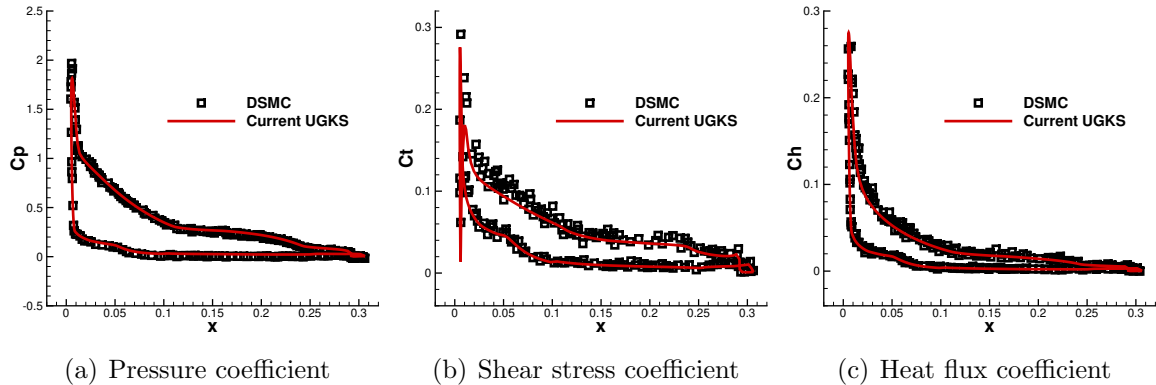


Figure 25: Surface quantities of hypersonic flow around an X38-like space vehicle at $\text{Mach}_\infty = 8.0$ and $\text{Kn}_\infty = 0.00275$ by the current UGKS program for argon gas compared with the DSMC method [67].

smaller memory footprint and faster computation speed. Table 1 shows the computation time and parallel efficiency for running 5,000 steps from 1 core to 512 cores. The parallel computing efficiency can be maintained above 70% when using fewer than 128 cores. When running the UGKS program, the computation time and parallel efficiency are shown in Table 2. The parallel efficiency is consistent with that of the GKS method, indicating that our program does not suffer from reduced parallel efficiency due to the multiple communications required at each step of the UGKS. Furthermore, for the computation with 64 cores, our new framework requires only 112.55 GB of memory, and for the computation with 512 cores, it requires 168.1227 GB of memory, making memory consumption no longer a bottleneck for the UGKS. The increase in memory is primarily due to the need for ghost cells for communication at parallel interfaces, necessitating extra memory to store the physical quantities of the ghost cells. However, this increase in memory is not significant relative to the rise in the number of cores, making it acceptable in computations. Compared to previous works, the GSIS [63] utilizes 512 cores and requires 1.32 TB of memory, which has about 3.28×10^{10} degrees of freedom with 961,080 hexahedral cells in the spatial discretization, 8,531 cells in the velocity space, and considering the vibrational freedoms. In contrast, the current UGKS program only consumes about 1/8 of the memory with the same number of cores for 9.63×10^9 (about 29.4%) degrees of freedom, indicating that we have greater memory usage efficiency.

5. Conclusion

In this paper, a parallel UGKS programming paradigm based on MPI is presented. Initially, the new strategy avoids storing the entire velocity space's slopes and residuals by implementing a two-step update method for the source term. Additionally, by leveraging the independent characteristics of the velocity space distribution functions, the reconstruction and update with a one-point offset are conducted, which reduce the number of MPI communications effectively through the utilization of non-blocking MPI communication.

The accuracy of the program is validated by testing cases, such as a three-dimensional lid-driven cavity flow, and hypersonic flows over a cylinder, a sphere, and an X38-like space

Table 1: Wall clock time and parallel computing efficiency of the GKS solver with 5,000 iterations in hypersonic flow around an X38-like space vehicle

Cores	Wall time (s)	Actual speedup	Parallel efficiency
1	10,091	1.00	100.00%
2	5,080	1.99	99.32%
4	2,632	3.83	95.85%
8	1,345	7.50	93.78%
16	701	14.40	89.97%
32	396	25.48	79.63%
64	207	48.75	76.17%
128	112	90.10	70.39%
256	69	146.25	57.13%
512	49	205.94	40.22%

Table 2: Wall clock time and parallel computing efficiency of the UGKS solver with 20 iterations in hypersonic flow around an X38-like space vehicle by the current UGKS program

Cores	Wall time (s)	Actual speedup	Parallel efficiency
64	2,257	1.00	100.00%
128	1,252	1.80	90.14%
256	698	3.23	80.84%
512	463	4.87	60.93%

vehicle. The program’s parallel efficiency is evaluated for both small-scale computations (three-dimensional lid-driven cavity flow) on a personal workstation and for large-scale computations (hypersonic flow around an X38-like space vehicle) on a supercomputing platform. The results indicate that the new programming paradigm achieves low memory consumption and high parallel efficiency. Notably, compared to previous methods like the GSIS [63], the current memory consumption is significantly reduced.

The computational efficiency of this program can be further improved by implementing implicit algorithms and adaptive velocity space strategies. Adopted with the current programming paradigm, efficient tools for simulating non-equilibrium flow can be developed in many other deterministic frameworks, such as DUGKS and GSIS.

Acknowledgements

We would like to thank Mr Cao Junzhe for discussion of the algorithm and the program design. This work was supported by the National Key R&D Program of China (Grant No. 2022YFA1004500) and the National Natural Science Foundation of China (Nos. 12172316 and 92371107), and the Hong Kong Research Grant Council (Nos. 16208021, 16301222, and 16208324).

References

- [1] G. A. Bird, *Molecular gas dynamics and the direct simulation of gas flows*, Oxford university press, 1994.
- [2] K. Xu, *A unified computational fluid dynamics framework from rarefied to continuum regimes*, Cambridge University Press, 2021.
- [3] S. D. Senturia, N. Azuru, J. White, Simulating the behavior of MEMS devices: computational methods and needs, *IEEE Computational Science and engineering* 4 (1) (1997) 30–43.
- [4] Y. Wang, S. Liu, C. Zhuo, C. Zhong, Investigation of nonlinear squeeze-film damping involving rarefied gas effect in micro-electro-mechanical systems, *Computers & Mathematics with Applications* 114 (2022) 188–209.
- [5] A. Alexeenko, D. Levin, S. Gimelshein, B. Reed, Numerical investigation of physical processes in high-temperature MEMS-based nozzle flows, in: *AIP conference proceedings*, Vol. 663, American Institute of Physics, 2003, pp. 760–767.
- [6] M. Wang, Z. Li, Simulations for gas flows in microgeometries using the direct simulation Monte Carlo method, *International Journal of Heat and Fluid Flow* 25 (6) (2004) 975–985.
- [7] G. Bird, Approach to translational equilibrium in a rigid sphere gas, *Phys. fluids* 6 (1963) 1518–1519.
- [8] G. Bird, Recent advances and current challenges for DSMC, *Computers & Mathematics with Applications* 35 (1-2) (1998) 1–14.
- [9] J. Fan, C. Shen, Statistical simulation of low-speed rarefied gas flows, *Journal of Computational Physics* 167 (2) (2001) 393–412.
- [10] C. Chu, Kinetic-theoretic description of the formation of a shock wave, *The Physics of Fluids* 8 (1) (1965) 12–22.
- [11] J. Yang, J. Huang, Rarefied flow computations using nonlinear model Boltzmann equations, *Journal of Computational Physics* 120 (2) (1995) 323–339.
- [12] L. Mieussens, Discrete-velocity models and numerical schemes for the Boltzmann-BGK equation in plane and axisymmetric geometries, *Journal of Computational Physics* 162 (2) (2000) 429–466.
- [13] F. Tcheremissine, Direct numerical solution of the Boltzmann equation, in: *AIP Conference Proceedings*, Vol. 762, American Institute of Physics, 2005, pp. 677–685.
- [14] K. Xu, J.-C. Huang, A unified gas-kinetic scheme for continuum and rarefied flows, *Journal of Computational Physics* 229 (20) (2010) 7747–7764.
- [15] Juan-Chen Huang, K. Xu, P. Yu, A unified gas-kinetic scheme for continuum and rarefied flows II: Multi-dimensional cases, *Communications in Computational Physics* 12 (3) (2012) 662–690.
- [16] C. Liu, Y. Zhu, K. Xu, Unified gas-kinetic wave-particle methods I: Continuum and rarefied gas flow, *Journal of Computational Physics* 401 (2020) 108977.
- [17] Y. Zhu, C. Liu, C. Zhong, K. Xu, Unified gas-kinetic wave-particle methods. II. multiscale simulation on unstructured mesh, *Physics of Fluids* 31 (6).
- [18] Z. Guo, K. Xu, R. Wang, Discrete unified gas kinetic scheme for all Knudsen number flows: Low-speed isothermal case, *Physical Review E-Statistical, Nonlinear, and Soft Matter Physics* 88 (3) (2013) 033305.
- [19] L. Yang, Z. Li, C. Shu, Y. Liu, W. Liu, J. Wu, Discrete unified gas-kinetic wave-particle method for flows in all flow regimes, *Physical Review E* 108 (1) (2023) 015302.
- [20] K. Xu, J.-C. Huang, An improved unified gas-kinetic scheme and the study of shock structures, *IMA Journal of Applied Mathematics* 76 (5) (2011) 698–711.
- [21] Sha Liu, P. Yu, K. Xu, C. Zhong, Unified gas-kinetic scheme for diatomic molecular simulations in all flow regimes, *Journal of Computational Physics* 259 (2014) 96–113.
- [22] Rui Zhang, S. Liu, C. Zhong, C. Zhuo, Unified gas-kinetic scheme with simplified multi-scale numerical flux for thermodynamic non-equilibrium flow in all flow regimes, *Communications in Nonlinear Science and Numerical Simulation* 119 (2023) 107079.
- [23] Zhao Wang, H. Yan, Q. Li, K. Xu, Unified gas-kinetic scheme for diatomic molecular flow with translational, rotational, and vibrational modes, *Journal of Computational Physics* 350 (2017) 237–259.

- [24] J.-C. Huang, K. Xu, P. Yu, A unified gas-kinetic scheme for continuum and rarefied flows III: Microflow simulations, *Communications in Computational Physics* 14 (5) (2013) 1147–1173.
- [25] C. Liu, K. Xu, A unified gas-kinetic scheme for micro flow simulation based on linearized kinetic equation, *Advances in Aerodynamics* 2 (1) (2020) 21.
- [26] L. Xu, W. Zhang, Y. Chen, R. Chen, A parallel discrete unified gas kinetic scheme on unstructured grid for inviscid high-speed compressible flow simulation, *Physics of Fluids* 34 (10) (2022) 106110.
- [27] L. Xu, Z. Yan, R. Chen, A discrete unified gas kinetic scheme on unstructured grids for viscous compressible flows and its parallel algorithm, *AIMS Mathematics* 8 (4) (2023) 8829–8846.
- [28] Y. Zhang, L. Zhu, P. Wang, Z. Guo, Discrete unified gas kinetic scheme for flows of binary gas mixture based on the McCormack model, *Physics of Fluids* 31 (1) (2019) 017101.
- [29] W. Sun, S. Jiang, K. Xu, G. Cao, Multiscale simulation for the system of radiation hydrodynamics, *Journal of Scientific Computing* 85 (2020) 1–24.
- [30] Jiang Song, X. Kun, S. Wenjun, X. Xiaojing, Unified gas kinetic schemes for the radiation transfer equations, *SCIENTIA SINICA Mathematica* 51 (6) (2021) 799.
- [31] C. Liu, K. Xu, Unified gas-kinetic wave-particle methods iv: multi-species gas mixture and plasma transport, *Advances in Aerodynamics* 3 (2021) 1–31.
- [32] M. Quan, X. Yang, Y. Wei, K. Xu, Radiative hydrodynamic equations with nonequilibrium radiative transfer, arXiv preprint arXiv:2409.01827.
- [33] S. Tan, Time implicit unified gas kinetic scheme for 3D multi-group neutron transport simulation, *Communications in Computational Physics* 28 (3) (2020) 1189–1218.
- [34] Z. Guo, K. Xu, Discrete unified gas kinetic scheme for multiscale heat transfer based on the phonon Boltzmann transport equation, *International Journal of Heat and Mass Transfer* 102 (2016) 944–958.
- [35] C. Zhang, R. Guo, M. Lian, J. Shiomi, Electron-phonon coupling and non-equilibrium thermal conduction in ultra-fast heating systems, *Applied Thermal Engineering* 249 (2024) 123379.
- [36] F. Fei, J. Zhang, J. Li, Z. Liu, A unified stochastic particle Bhatnagar–Gross–Krook method for multiscale gas flows, *Journal of Computational Physics* 400 (2020) 108972.
- [37] F. Fei, Y. Ma, J. Wu, J. Zhang, An efficient algorithm of the unified stochastic particle Bhatnagar–Gross–Krook method for the simulation of multi-scale gas flows, *Advances in Aerodynamics* 3 (2021) 1–16.
- [38] Z. Guo, J. Li, K. Xu, Unified preserving properties of kinetic schemes, *Physical Review E* 107 (2) (2023) 025301.
- [39] R. Yuan, C. Zhong, A conservative implicit scheme for steady state solutions of diatomic gas flow in all flow regimes, *Computer Physics Communications* 247 (2020) 106972.
- [40] T. Xiao, C. Liu, K. Xu, Q. Cai, A velocity-space adaptive unified gas kinetic scheme for continuum and rarefied flows, *Journal of Computational Physics* 415 (2020) 109535.
- [41] Y. Wei, W. Long, K. Xu, Adaptive unified gas-kinetic scheme for diatomic gases with rotational and vibrational nonequilibrium, *Computer Physics Communications* 305 (2024) 109324.
- [42] L. Yang, L. Han, H. Ding, Z. Li, C. Shu, Y. Liu, Adaptive partitioning-based discrete unified gas kinetic scheme for flows in all flow regimes, *Advances in Aerodynamics* 5 (1) (2023) 15.
- [43] Y. Wei, J. Cao, X. Ji, K. Xu, Adaptive wave-particle decomposition in UGKWP method for high-speed flow simulations, *Advances in Aerodynamics* 5 (1) (2023) 25.
- [44] Y. Zhu, C. Zhong, K. Xu, Implicit unified gas-kinetic scheme for steady state solutions in all flow regimes, *Journal of Computational Physics* 315 (2016) 16–38.
- [45] Y. Zhu, C. Zhong, K. Xu, An implicit unified gas-kinetic scheme for unsteady flow in all Knudsen regimes, *Journal of Computational Physics* 386 (2019) 190–217.
- [46] R. Zhang, S. Liu, J. Chen, C. Zhuo, C. Zhong, A conservative implicit scheme for three-dimensional steady flows of diatomic gases in all flow regimes using unstructured meshes in the physical and velocity spaces, *Physics of Fluids* 36 (1).
- [47] W. Long, Y. Wei, K. Xu, An implicit adaptive unified gas-kinetic scheme for steady-state solutions of nonequilibrium flows, *Physics of Fluids* 36 (10) (2024) 106114.
- [48] S. Li, Q. Li, S. Fu, K. Xu, A unified gas-kinetic scheme for axisymmetric flow in all Knudsen number

- regimes, *Journal of Computational Physics* 366 (2018) 144–169.
- [49] W. T. Taitano, D. A. Knoll, L. Chacón, J. M. Reisner, A. K. Prinja, Moment-based acceleration for neutral gas kinetics with BGK collision operator, *Journal of Computational and Theoretical Transport* 43 (1-7) (2014) 83–108.
- [50] L. Chacon, G. Chen, D. A. Knoll, C. Newman, H. Park, W. Taitano, J. A. Willert, G. Womeldorff, Multiscale high-order/low-order (HOLO) algorithms and applications, *Journal of Computational Physics* 330 (2017) 21–45.
- [51] S. Chen, C. Zhang, L. Zhu, Z. Guo, A unified implicit scheme for kinetic model equations. part I. memory reduction technique, *Science bulletin* 62 (2) (2017) 119–129.
- [52] L. Yang, C. Shu, W. Yang, J. Wu, An implicit scheme with memory reduction technique for steady state solutions of DVBE in all flow regimes, *Physics of Fluids* 30 (4).
- [53] C. Mouhot, L. Pareschi, Fast algorithms for computing the Boltzmann collision operator, *Mathematics of computation* 75 (256) (2006) 1833–1852.
- [54] L. Wu, C. White, T. J. Scanlon, J. M. Reese, Y. Zhang, Deterministic numerical solutions of the Boltzmann equation using the fast spectral method, *Journal of Computational Physics* 250 (2013) 27–52.
- [55] S. Chen, K. Xu, C. Lee, Q. Cai, A unified gas kinetic scheme with moving mesh and velocity space adaptation, *Journal of Computational Physics* 231 (20) (2012) 6643–6664.
- [56] M. T. Ho, L. Zhu, L. Wu, P. Wang, Z. Guo, Z.-H. Li, Y. Zhang, A multi-level parallel solver for rarefied gas flows in porous media, *Computer Physics Communications* 234 (2019) 14–25.
- [57] D. Jiang, M. Mao, J. Li, X. Deng, An implicit parallel UGKS solver for flows covering various regimes, *Advances in Aerodynamics* 1 (2019) 1–24.
- [58] C. Baranger, J. Claudel, N. Hérouard, L. Mieussens, Locally refined discrete velocity grids for deterministic rarefied flow simulations, in: *AIP Conference Proceedings*, Vol. 1501, American Institute of Physics, 2012, pp. 389–396.
- [59] S. Li, Q. Li, S. Fu, J. Xu, The high performance parallel algorithm for unified gas-kinetic scheme, in: *AIP Conference Proceedings*, Vol. 1786, AIP Publishing, 2016.
- [60] T. Shuang, S. Wenjun, W. Junxia, N. Guoxi, A parallel unified gas kinetic scheme for three-dimensional multi-group neutron transport, *Journal of Computational Physics* 391 (2019) 37–58.
- [61] Q. Zhang, Y. Wang, D. Pan, J. Chen, S. Liu, C. Zhuo, C. Zhong, Unified x-space parallelization algorithm for conserved discrete unified gas kinetic scheme, *Computer Physics Communications* 278 (2022) 108410.
- [62] P. Wang, J. Li, D. Jiang, M. Mao, Parallel implementation and verification of implicit unified gas kinetic scheme, in: *2022 6th High Performance Computing and Cluster Technologies Conference (HPCCT)*, ACM, Fuzhou China, 2022, pp. 25–30.
- [63] Y. Zhang, J. Zeng, R. Yuan, W. Liu, Q. Li, L. Wu, Efficient parallel solver for rarefied gas flow using GSIS, *Computers & Fluids* 281 (2024) 106374.
- [64] K. Xu, Direct modeling for computational fluid dynamics, *Acta Mechanica Sinica* 31 (2015) 303–318.
- [65] Y. Zhang, X. Ji, K. Xu, A high-order compact gas-kinetic scheme in a rotating coordinate frame and on sliding mesh, *International Journal of Computational Fluid Dynamics* (2023) 1–20.
- [66] L. Yang, C. Shu, W. Yang, J. Wu, An improved three-dimensional implicit discrete velocity method on unstructured meshes for all Knudsen number flows, *Journal of Computational Physics* 396 (2019) 738–760.
- [67] J. Li, D. Jiang, X. Geng, J. Chen, Kinetic comparative study on aerodynamic characteristics of hypersonic reentry vehicle from near-continuous flow to free molecular flow, *Advances in Aerodynamics* 3 (2021) 1–10.
- [68] K. Xu, A gas-kinetic BGK scheme for the Navier–Stokes equations and its connection with artificial dissipation and Godunov method, *Journal of Computational Physics* 171 (1) (2001) 289–335.